Sequence-Specific Solution Structure of d-GGTACGCGTACC

K. V. R. Chary, R. V. Hosur, and Girjesh Govil*

Chemical Physics Group, Tata Institute of Fundamental Research, Homi Bhabha Road, Bombay 400005, India

Chang-qing Chen and H. Todd Miles*

Laboratory of Molecular Biology, National Institute of Diabetes and Digestive and Kidney Diseases, National Institutes of Health, Bethesda, Maryland 20892

Received October 8, 1987; Revised Manuscript Received January 13, 1988

ABSTRACT: Complete resonance assignments of nonexchangeable base protons and sugar protons in d-GGTACGCGTACC at 500 MHz have been obtained by two-dimensional correlated spectroscopy (COSY) and nuclear Overhauser enhancement spectroscopy (NOESY). The characteristic phase-sensitive multiplet patterns of the intrasugar cross peaks in the ω_1-scaled COSY spectrum have been used to estimate several scalar coupling constants (J). These coupling constants combined with the intranucleotide COSY cross peak intensities have been used to identify the sugar pucker of individual nucleotide units. In most cases, the deoxyribose rings adopt a conformation close to O4'-endo. Spin-diffusion has been monitored from the buildup of the normalized volumes of NOE cross peaks in NOESY spectra as a function of mixing time. A set of 55 intranucleotide and internucleotide interproton distances have been estimated from the low mixing time NOESY spectrum (τ_m = 75 ms). The estimated intranucleotide proton–proton distances have been used to determine the individual glycosidic dihedral angles of the nucleotide units which lie in the anti domain. It is observed that the molecule adopts an overall conformation close to that of the B-form although there are differences in the intricate details.

We have been working toward obtaining accurate solution structures of protein binding segments of DNA using two-dimensional NMR techniques, with a view to understanding DNA structure and the role it plays in specific recognition between proteins and nucleic acids. The methodologies are being improved to obtain data of better quality (Hosur et al., 1985a,b, 1987a,b), and new strategies are being developed to obtain more precise and detailed structural information from the experimental spectra. Low-resolution structures have been obtained earlier for the following double-helical DNA segments: (I) d-GGATCCGGATCC (Hosur et al., 1985; Ravikumar et al., 1985); (II) d-GAATTCGAATTC (Chary et al., 1987; Hosur et al., 1986a); (III) d-CTCGAGCTCGAG (Sheth et al., 1987a); (IV) d-GAATTCCCGAATTC (Hosur et al., 1986b); (V) d-$(CG)_6$ (Sheth et al., 1987b). Among these, I–IV have recognition sites for the restriction enzymes *Bam*HI, *Eco*RI, *Xho*I, and *Eco*RI, respectively. In all cases it has been observed that while the molecules adopt an overall B-DNA structure, the cleavage sites on the oligonucleotides exhibit significant conformational variations compared to the remaining part of the respective molecules. At the level that these structures have been determined, only qualitative statements could be made about the backbone structure and glycosidic dihedral angles. A better characterization of the sequence-dependent structural variations requires more precise determination of the structure. The structure quality can be improved by quantitative estimates of the intrasugar proton–proton coupling constants (J) and interproton distances (r) within the molecules (Kumar et al., 1981; Chazin et al., 1986; Hare et al., 1986a,b; Hosur et al., 1987b).

In this paper, we report sequence-specific ^{1}H resonance assignments and estimation of ring proton–proton coupling constants and of interproton distances in d-GGTACGCGTACC (VI) by making use of the two-dimensional (2D) NMR techniques two-dimensional correlated spectroscopy (COSY), ω_1-scaled COSY, and nuclear Overhauser enhancement spectroscopy (NOESY). d-GGTACGCGTACC is a variant of I. The difference between I and VI is the sequence alteration of the underlined segments. This molecule (VI) has specific cleavage sites for the restriction endonuclease *Rsa*I and *Fnu*DII (Figure 1). The former enzyme recognizes the GTAC fragment and cleaves between T and A whereas the latter one recognizes the CGCG fragment and cleaves between G and C in the middle of the sequences recognized.

Materials and Methods

Synthesis. d-GGTACGCGTACC was prepared by a manual method developed for relatively large-scale synthesis (e.g., 30–80 mg of purified product) of DNA fragments (C.-q. Chen, J. Frazier, and H. T. Miles, unpublished experiments). The oligonucleotides were assembled on a controlled pore glass (CPG) support with cyanoethyl phosphoramidite chemistry (McBride & Caruthers, 1983; Sinha et al., 1984; Atkinson & Smith, 1984). The method employed a unidirectional flow of reagents under argon pressure through a CPG-filled column. Average coupling efficiency was about 97%. The oligomer was purified by DEAE-cellulose chromatography with a 0–0.8 M gradient of ammonium bicarbonate at atmospheric pressure, with 7 M urea to prevent self-association (Staehelin et al., 1959; Tomlinson & Tener, 1963). The purified product was homogeneous on HPLC (0.02 TEAE–acetonitrile 0–50% gradient) and 20% acrylamide gel containing 8 M urea.

Sample Preparation. For the ^{1}HNMR experiments on d-GGTACGCGTACC, 6 mg of the sample was dissolved in 400 μL of 50 mM sodium phosphate buffer (pH 7.3) and 1 mM ethylenediaminetetraacetic acid (EDTA). Such a solution was repeatedly lyophilized from ^2H_2O solution. Finally, the sample was made up to 0.4 mL with 99.7% ^2H_2O for the NMR experiments in ^2H_2O. For detection of exchangeable imino proton resonances, the same sample was dissolved in water, lyophilized, and finally made up to 0.4 mL with a mixture

0006-2960/88/0427-3858$01.50/0

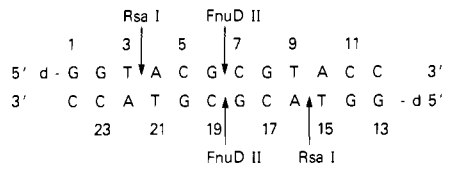

FIGURE 1: Preferential cleavage sites for restriction endonucleases *Rsa*I and *Fnu*DII in double-helical d-GGTACGCGTACC (VI). The corresponding recognition segments are GTAC and CGCG, respectively.

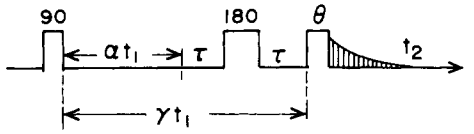

FIGURE 2: Pulse sequence for phase-sensitive ω_1-scaled COSY. α and γ are the chemical shift and J-scaling factors, respectively. τ is a delay which changes with t_1, and θ is the flip angle of the mixing pulse. This has been fixed equal to $\pi/2$ in the present studies.

consisting of 80% H_2O and 20% ^2H_2O.

Nuclear Magnetic Resonance Spectroscopy. All ^1H spectra of GGTACGCGTACC were recorded on a Bruker AM-500 FT NMR spectrometer equipped with an ASPECT 3000 computer. The spectrum in H_2O was recorded with a 1–3–3–1 selective excitation pulse sequence for water suppression (Hore, 1983). COSY data were recorded with a RD–90°–t_1–Δ–90°–Δ–t_2 pulse sequence, where Δ is the fixed delay (5 ms) used for the enhancements of cross peaks (Bax & Freeman, 1981; Kumar et al., 1984; Hosur et al., 1985c; Wynants & Van Binst, 1984). The carrier was placed at one end, and quadrature detection was used in t_2. The time domain data set consisted of 2048 and 512 data points along the t_2 and t_1 domains, respectively. The number of transients collected for each t_1 value was 64. The data set was zero filled to 1024 along the t_1 axis and was multiplied by unshifted sine square bell and unshifted sine bell window functions along the t_2 and t_1 axes, respectively, before two-dimensional Fourier transformation. The digital resolution along both the axes was 7.5 Hz/point.

A phase-sensitive ω_1-scaled COSY (Hosur et al., 1985a, 1987b) spectrum was recorded with the pulse sequence shown in Figure 2. This pulse sequence provides chemical shift scaling by a factor α and J-scaling by a factor γ along the ω_1 axis of the 2D spectrum. In the present case, α and γ were chosen as 0.5 and 1.5, respectively, for the purpose of enhancement of the resolution between the individual components of the characteristic phase-sensitive multiplet patterns of the cross peaks. The time domain data set consisted of 2048 and 320 data points along t_2 and t_1 domains, respectively. The number of transients collected for each t_1 value was 160. The spectral offset was placed at the center of the spectrum. The data set was zero filled to 4096 and 2048 along the t_2 and t_1 axes and was multiplied by sine bells (shifted by $\pi/16$) along both axes before two-dimensional Fourier transformation. The digital resolution along both the axes was 1.8 Hz/point.

Absorption mode NOESY (Marion & Wüthrich, 1983) spectra of the dodecamer in ^2H_2O solution were recorded under identical conditions at several mixing times, viz., 300, 200, 150, 100, 75, and 50 ms, with a repetition delay of 1.2 s and the standard NOESY pulse sequence. In each of these experiments, the spectral offset was placed at the center of the spectrum, and the number of transients collected for each t_1 value was 64. The time domain data sets were collected with 2048 and 512 data points along the t_2 and t_1 dimensions. These data sets were zero filled to 2048 data points along the t_1 axis and multiplied by Lorentz–Gaussian window functions (LB = –2 Hz; GB = 0.05 Hz) along both the axes before the two-dimensional Fourier transformation. The resultant digital resolution along both of the axes was 3.7 Hz/point.

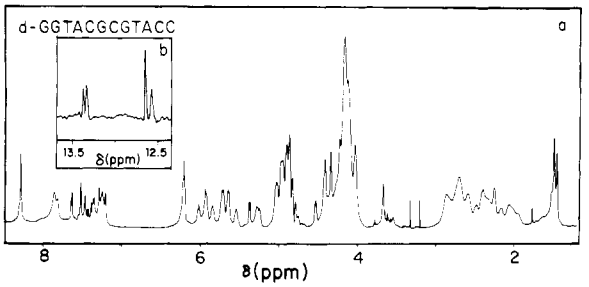

FIGURE 3: One-dimensional 500-MHz ^1H NMR spectra of (a) nonexchangeable and (b) exchangeable protons in d-GGTACGCGTACC recorded as a 5 mM solution in ^2H_2O and as a 5 mM solution in 80% H_2O + 20% ^2H_2O (pH 7.2), respectively, at 25 °C. Spectrum b was obtained with the 1–3–3–1 selective excitation pulse sequence.

The spectra were recorded at 25 °C. The melting temperature of VI has been determined to be 60 °C in 0.1 M Na^+ from IR experiments. The temperature of measurements therefore is in the range where VI is in an ordered conformation.

Results and Discussion

Resonance Assignment. Figure 3 shows 500-MHz ^1H NMR spectra of (a) nonexchangeable and (b) exchangeable imino protons of d-GGTACGCGTACC recorded from ^2H_2O and 80% H_2O + 20% ^2H_2O solutions. Sequence-specific assignment of nonexchangeable protons has been obtained following well-established procedures (Clore & Gronenborn, 1985; Feigon et al., 1982, 1983; Frechet et al., 1983; Hare et al., 1983; Hosur et al., 1985a; Reid et al., 1983; Scheek et al., 1983, 1984). In the first step, a COSY spectrum is used to identify the sugar protons belonging to the individual networks of coupled spins. The cytidine and thymidine base protons are identified with J(H5, H6) and $J(CH_3–H_6)$ correlations. In the next step, the intranucleotide and internucleotide NOEs between the base protons (H6, H8, and CH_3) and the sugar protons (H1′, H2′, and H2″) in the NOESY spectrum are used to assign the above networks to individual units. In the present study, three different types of sequential correlations have been observed, namely, $(base)_i \rightarrow (base)_{i\pm1}$ (d_1), $(base)_i \rightarrow (H1')_{i-1}$ (d_2), and $(base)_i \rightarrow (H2', H2'')_{i-1}$ (d_3). As an illustration, Figure 4 shows some of the d_1, d_2, and d_3 connectivities. Stereospecific assignment of the H2′, H2″ protons has been obtained from the NOESY spectrum by monitoring the intensities of H1′–(H2′, H2″) cross peaks. H1′–H2″ cross peaks are invariably stronger than H1′–H2′ peaks as discussed in previous papers (Chary et al., 1987; Hosur et al., 1986b). The assignments of H3′ and H4′ protons have been carried out through the concerted use of H2′–H3′, H3′–H4′ J correlations in COSY and $(base)_i - (H3')_i$, $(H1')_i - (H4')_i$ distance correlations (Figure 4) in the NOESY spectrum. The efficient spin-diffusion occurring among the sugar protons of individual nucleotide units results in the observation of $(base\ H8/H6)_i$–$(H5', H5'')_i$ and $(H1')_i$–$(H5', H5)_i$ NOESY cross peaks (Figure 5). This has been utilized for assigning most of the H5′, H5″ sugar protons. The above-mentioned assignments are listed in Table I in terms of the chemical shifts of various protons.

3D Structure of the Oligonucleotide. Observation of four resonance lines in the imino proton region (11–14 ppm) of the one-dimensional NMR spectrum (Figure 3b) confirms the results from UV and IR measurements (F. B. Howard, C.-q.

Table I: Chemical Shifts of Nonexchangeable Protons in d-GGTACGCGTACC Expressed with Respect to Sodium 3-(Trimethylsilyl)[2,2,3,3-$^2H_4$]propionate ([^{2}H]TSP)

unit	H1′	H2′	H2″	H3′	H4′	H5′, H5″	H6/H8	H5/CH_3/H2
G1	5.68	2.56	2.64	4.78			7.34	
G2	6.00	2.64	2.80	4.95	4.37	4.14, 4.20	7.85	
T3	5.67	2.12	2.46	4.86	4.21	4.13, 4.21	7.27	1.43
A4	6.18	2.69	2.85	5.00	4.40	4.09, 4.13	8.26	7.49
C5	5.51	1.89	2.28	4.80	4.21		7.22	5.23
G6	5.82	2.54	2.68	4.79	4.12	4.06, 4.13	7.81	
C7	5.61	1.95	2.35	4.82	4.14		7.24	5.26
G8	5.91	2.59	2.76	4.91	4.31	4.06, 4.13	7.85	
T9	5.63	2.01	2.36	4.82	4.14	4.10, 4.15	7.18	1.47
A10	6.18	2.69	2.85	5.00	4.40	4.09, 4.13	8.26	7.45
C11	5.92	2.04	2.36	4.73	4.15	4.10, 4.13	7.34	5.36
C12	6.19	2.23	2.26	4.50	4.00		7.61	5.72

Chen, J. Frazier, and H. T. Miles, unpublished experiments) that the molecule forms a double helix. Observations of two interstrand NOEs (H2 of A4 to H1′ of A10 on the opposite strand and H2 of A10 to H1′ of A4; Figure 4) confirm the duplex structure and intact AT pairs. The directionality of these NOEs further establishes the right-handed sense of the helix [cf. Hare et al. (1986a)].

A more precise quantitative description of the 3D structure of the oligomer requires the knowledge of the proton–proton scalar coupling constants (J) and the proton–proton distances (r) which can be obtained from the 2D NMR techniques. While considering either of these basic inputs, one has to keep in mind the dynamics of the molecule. The observed parameters are time averages, and therefore, the data will have to be analyzed in terms of contributions from individual conformers.

Estimation of Scalar Coupling Constants (J). There are six proton–proton coupling constants (J) in each deoxyribose ring, namely, H1′–H2′, H2′–H2″, H2′–H3′, H2″–H3′, and H3′–H4′. One of these, H2′–H2″, is a two-bond geminal coupling. The value of this coupling constant is around −14 Hz and does not show significant conformation-dependent variations. The other five J values are three-bond vicinal couplings which show very strong dependence on the conformation of the deoxyribose ring. The conformational dependence of these J values has been established [see, for example, Chary et al., (1987), Hosur et al. (1986a,b), Sheth et al. (1987b), and Rinkel and Altona (1987)]. Table II lists expected J values for some selected conformations for the convenience of the discussion in this paper, along with the experimental results. In our earlier work we have utilized the qualitative features of such J values and their influence on the low-resolution COSY patterns to fix the sugar geometries in oligonucleotides I–V. Our argument has been that, under the low-resolution conditions of the observations of such data, the intensity of the cross peak is indicative of the approximate magnitude of the corresponding J value. Here, we describe methods to obtain more quantitative information.

Experimental quantification of the J values for the deoxyribose rings is a very difficult task. In the phase-sensitive COSY spectrum, the cross peaks have geometry-dependent complex multiplet patterns. For example, the H1′–H2′, H1′–H2″, and H2′–H3′ cross peaks will generally have 4 × 8, 4 × 4, and 8 × 8 multiplet components, respectively. Recently it has been shown that the incorporation of ω_1 scaling (Chazin et al., 1986; Hosur et al., 1985d, 1987a,b) improves the resolution significantly. Thus using this technique, we have been able to resolve the individual components of the H1′–H2″ phase-sensitive cross peaks in all the nucleotide units of VI, except in C12 where H2′ and H2″ show very small chemical shift dispersion. The patterns have been analyzed to obtain

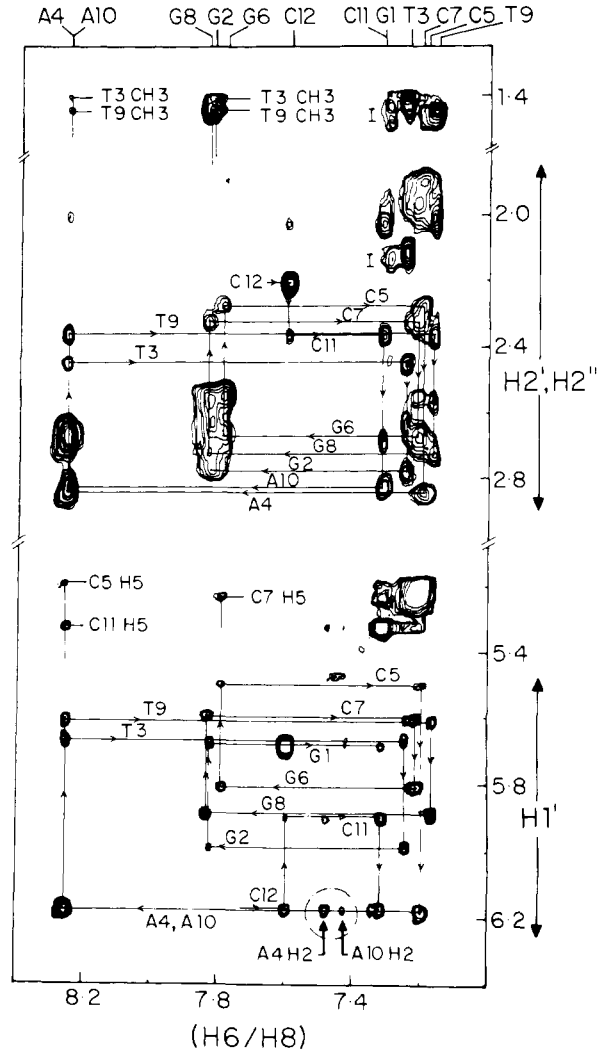

FIGURE 4: Expansion of selected regions of phase-sensitive NOESY spectrum recorded with τ_m = 200 ms. Sequential connectivities using base H6/H8 protons and H1′ sugar protons (d_2 pathways), base H6/H8 protons and H2′/H2″ sugar protons (d_3 pathways), and base H6/H8 protons to base H5/CH_3 protons (d_1 pathways) are shown in this figure. This figure also contains interstrand internucleotide NOESY connectivities, which are shown with dark arrows.

values of J(H1′–H2′), J(H1′–H2″), J(H2′–H2″), and J-(H2″–H3′). The analysis involved is briefly described below.

The features of the phase-sensitive COSY spectrum depend on the relative values of coupling constants involved, which in turn are governed by the sugar pucker. Figures 6 and 7 show the expected patterns of the H1′–H2″ and H1′–H2′ cross peaks for two sugar puckers: C2′-endo (P = 162°) and O4′-endo (P = 90°). Patterns for other sugar geometries can

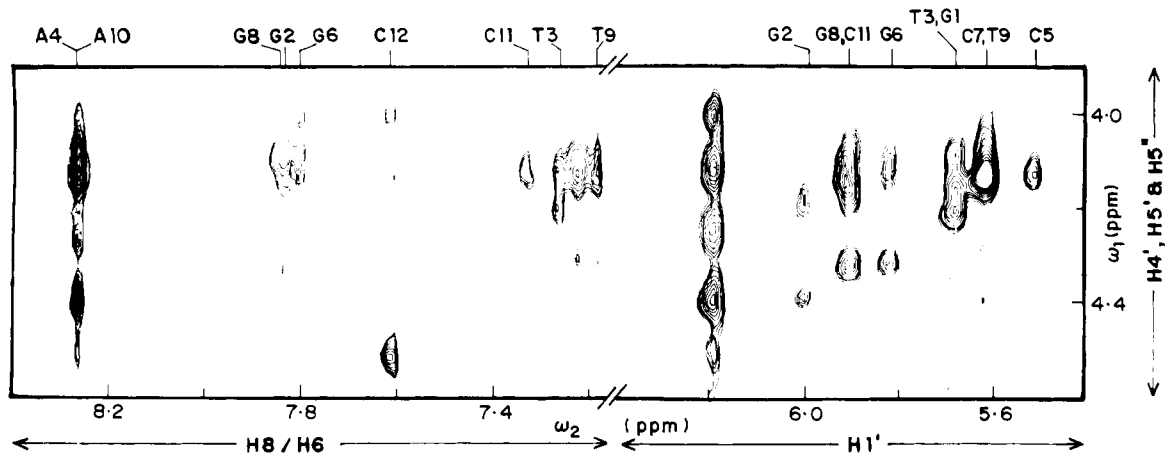

FIGURE 5: Selected region of the NOESY spectrum of d-GGTACGCGTACC recorded with τ_m = 200 ms. This figure shows the NOESY cross peaks from base H6/H8 protons and sugar H1′ protons to H4′, H5′, and H5″ protons belonging to the same nucleotide unit, which have been used to assign some of the H4′, H5′, and H5″ protons.

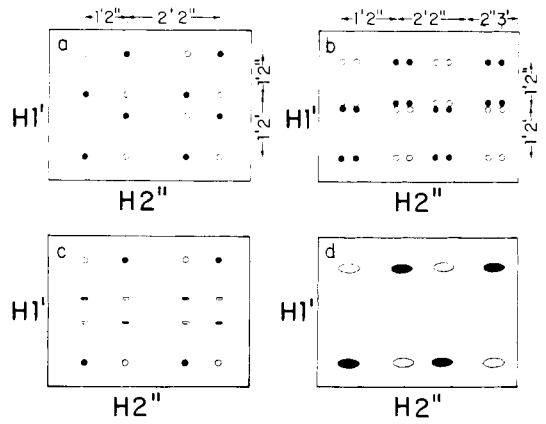

FIGURE 6: Expected characteristic phase-sensitive multiplet patterns of the H1′–H2″ cross peak. (○) Positive phase; (●) negative phase. (a) In the case of C2′-endo geometry, with infinite resolution, the pattern has been simulated with J(H1′–H2″) = 9 Hz, J(H1′–H2″) = 7 Hz, J(H2″–H3′) = 0 Hz, and J(H2′–H2″) = −14 Hz. (b) In the case of O4′-endo geometry, with infinite resolution, the pattern has been simulated with J(H1′–H2′) = 7 Hz, J(H1′–H2″) = 8 Hz, J(H2″–H3′) = 2 Hz, and J(H2′–H2″) = −14 Hz. (c) Same as (a) but with a digital resolution of 2 Hz/point. (d) Same as (b) but with a digital resolution of 2 Hz/point.

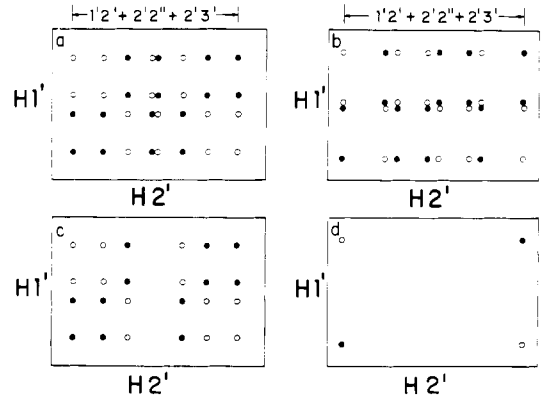

FIGURE 7: Expected characteristic phase-sensitive multiplet patterns of the H1′–H2′ cross peak. (○) Positive phase; (●) negative phase. (a) In the case of C2′-endo geometry, with infinite resolution, the pattern was simulated with J(H1′–H2′) = 9 Hz, J(H1′–H2″) = 6 Hz, J(H2′–H3′) = 6 Hz, and J(H2′–H2″) = −14 Hz. (b) In the case of O4′-endo geometry, with infinite resolution, the pattern was simulated with J(H1′–H2′) = 7 Hz, J(H1′–H2″) = 8 Hz, J(H2′–H3′) = 9 Hz, and J(H2′–H2″) = −14 Hz. (c) Same as (a) but with a digital resolution of 2 Hz/point. (d) Same as (b) but with a digital resolution of 2 Hz/point.

be easily simulated with the theoretically estimated J values. Under the best possible conditions of digital resolution (2 Hz/point), the experimental patterns for the H1′–H2″ cross peaks will appear as illustrated in Figure 6c,d. The resultant patterns are the combined results of line widths, small values of J(H2″–H3′), and small differences in the value of J(H1′–H2′) and J(H1′–H2″). In the case of C2′-endo geometry, all the multiplet components are expected to be resolved, and the measurement of J(H1′–H2′), J(H1′–H2″), and J(H2′–H2″) from the experimental spectra is straightforward (Figure 6c). On the other hand, if one is dealing with O4′-endo geometry (Figure 6d), then a small but nonzero value of J(H2″–H3′) would be buried in the line widths, and its effect will be simply to elongate the individual components in the cross peaks (Figure 6d). However, one can accurately measure J(H1′–H2″) and J(H2′–H2″) along the ω_2 axis, since the centers of the peaks are not affected. Along the ω_1 axis of the same cross peak, the largest separation corresponds to the sum of J(H1′–H2′) and J(H1′–H2″). Hence, the value of J(H1′–H2′) can be obtained with the already-known value of J(H1′–H2″). In either of the two sugar puckers considered here, the value of J(H2″–H3′) is too small to be resolved under the experimental conditions. However, the experimental resolution can be used to fix an upper limit for this J value. It is also easy to realize that the experimental pattern will be very different if one is dealing with a conformer in the N domain (i.e., C3′-endo). Figure 8 shows the H1′–(H2′, H2″) region of the experimental ω_1-scaled phase-sensitive COSY spectrum of the present oligonucleotide d-GGTACGCGTACC. The boxed sets of cross peak patterns in the figure show the characteristic phase-sensitive multiplets of the H1′–H2″ cross peaks belonging to different nucleotide units. The peaks corresponding to H1′–H2′ are in the unboxed sets. For a particular nucleotide, these lie in the same horizontal area to the right of the boxed H1′–H2″ peaks and can be identified with the chemical shift for the H2′ proton from Table I. Both the positive and the negative phases are monitored individually, but this has been shown only for C11 for clarity. It may be noted here that the chemical shifts of H1′, H2′, and H2″ of A4 are identical with the respective chemical shifts of A10, and therefore, only one set of cross peaks is seen, representing both of them.

It is seen that the cross peak patterns for H1′–H2″ resemble the ones shown in Figure 6d. The ω_2 axis contains the information about J(H1′–H2″), J(H2′–H2″), and J(H2″–H3′). J(H2″–H3′) is buried in the line widths and hence can be considered to be less than ca 3 Hz. The ω_1 axis has the

Table II: Experimentally Observed and Theoretically Expected Values of Scalar Coupling Constants (J in Hertz) in the Sugar Rings of d-GGTACGCGTACC[a]

residue	H1′–H2′	H1′–H2″	H2′–H3′	H2″–H3′	H3′–H4′	H2′–H2″
			(a) Experimental Values			
G1	9.7	7.0	m	w; <3	a	14.5
G2	9.0	8.2	m	w; <3	m	13.5
T3	9.0	7.7	m	a; <3	m	14.1
A4	8.7	7.5	m	o; <3	m	14.1
C5	8.7	7.5	w	a; <3	m	14.0
G6	9.0	7.7	w	a; <3	m	14.1
C7	9.0	7.7	m	a; <3	m	14.1
G8	9.0	7.7	m	a; <3	m	14.1
T9	9.0	7.7	m	a; <3	m	14.1
A10	8.7	7.5	m	o; <3	m	14.1
C11	8.7	7.5	m	m; <3	m	14.5
C12	s	s	s	o	s	o
			(b) Theoretical Values for Selected Conformations			
C3′-endo	0	8	6	9	9	
O4′-endo	7	8	9	3	7	
C1′-exo	9.5	6	8	0	3	
C2′-endo	9.5	6	6	0	0	

[a] Estimates of J(H2′–H3′) and J(H3′–H4′) are based on the intensity of the respective cross peaks in the low-resolution COSY spectrum. a = peak absent (very small J); w = weak peak (small J); m = medium peak (moderately large J); s = strong (large J); o = peaks overlap. The values of J(H1′–H2′) and J(H1′–H2″) are obtained from the phase-sensitive multiplet patterns of the intrasugar cross peaks in the ω_1-scaled COSY spectrum. Values of J(H2″–H3′) are below the resolution of the phase-sensitive COSY, and this fact is independently confirmed by the low-resolution COSY peak intensities. The sign of J(H2′–H2″) is negative. The pseudorotational phase angle P is 18° for C3′-endo geometry (N domain) and 90°, 126°, and 162° respectively, for the three S domain conformations O4′-endo, C1′-exo, and C2′ endo used in the analysis in the text. Accuracy of experimental coupling constants measured is ±0.3 Hz. Theoretical values have been calculated with Karplus-type relation [see Hosur et al. (1986a)].

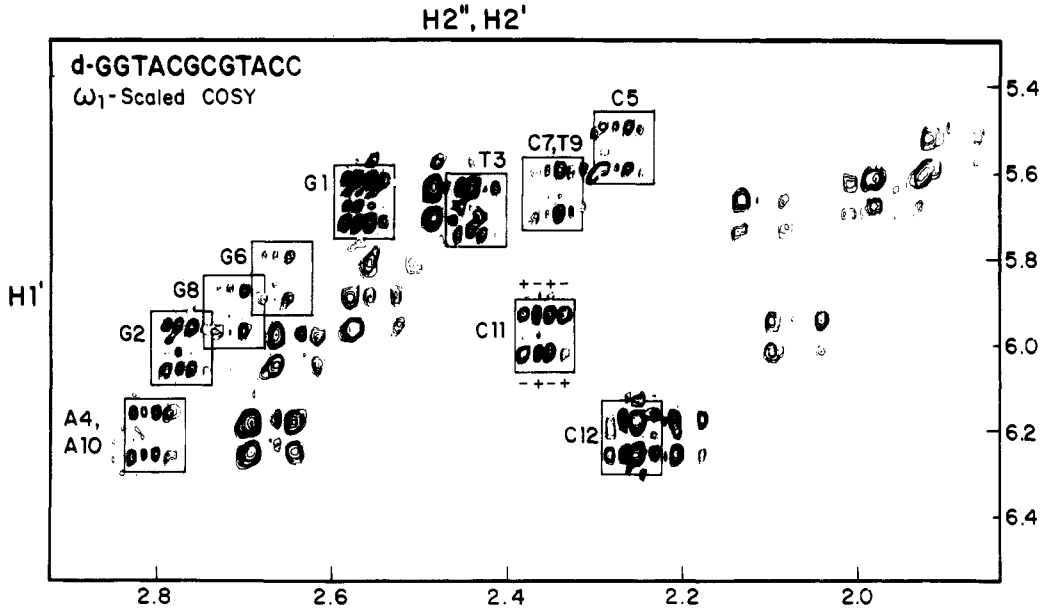

FIGURE 8: Selected region of 500-MHz ω_1-scaled phase-sensitive COSY spectrum of d-GGTACGCGTACC recorded in ^2H_2O at 25 °C. This figure covers all the expected H1′–H2′ and H1′–H2″ cross peaks. The positive and negative levels of the cross peaks are monitored in these spectra. For example, positive and negative levels are depicted as (+) and (−), respectively, in the case of the H1′–H2″ cross peak of the C11 nucleotide unit. Boxed portions in this figure show the characteristic phase-sensitive multiplet patterns of H1′–H2″ cross-peaks belonging to different nucleotide units. Unboxed portions depict all the expected H1′–H2′ cross peak multiplet patterns. The digital resolution along the ω_1 and ω_2 axes is 1.9 Hz/point.

information on $|J$(H1′–H2′) + J(H1′–H2″)|. The values of the measured coupling constants are listed in Table II. In the case of C12, the resonances of H2′ and H2″ are not dispersed enough at the available digital resolution, and hence, the corresponding J values could not be estimated.

Information on J(H2′–H3′) can in principle be obtained from the multiplicity pattern of the H1′–H2′ cross peaks. As an example, we have shown the expected patterns of such cross peaks for the C2′-endo (P = 162°) and O4′-endo (P = 90°) sugar geometries (Figure 7). Under the achievable conditions of digital resolution (2 Hz/point), the experimental patterns will appear as in panels c and d of Figure 7, respectively. Along the ω_2 axis, the cross peak has the information about J(H1′–H2′), J(H2′–H2″), and J(H2′–H3′). The separation between the farthest components corresponds to the sum of these values. With the knowledge of J(H1′–H2′) and J(H2–H2″) estimated earlier, the value of J(H2′–H3′) can be discerned in favorable cases.

The unboxed portions of Figure 8 depict characteristic phase-sensitive multiplet patterns of the H1′–H2′ cross peaks belonging to different nucleotide units. Each of these cross peaks has only four lobes instead of the expected 4 × 8 pattern. Hence, in the present oligonucleotide the value of J(H2′–H3′) could not be measured accurately.

Estimation of J(H3′–H4′) requires good resolution in the respective cross peak region of the phase-sensitive COSY. Due

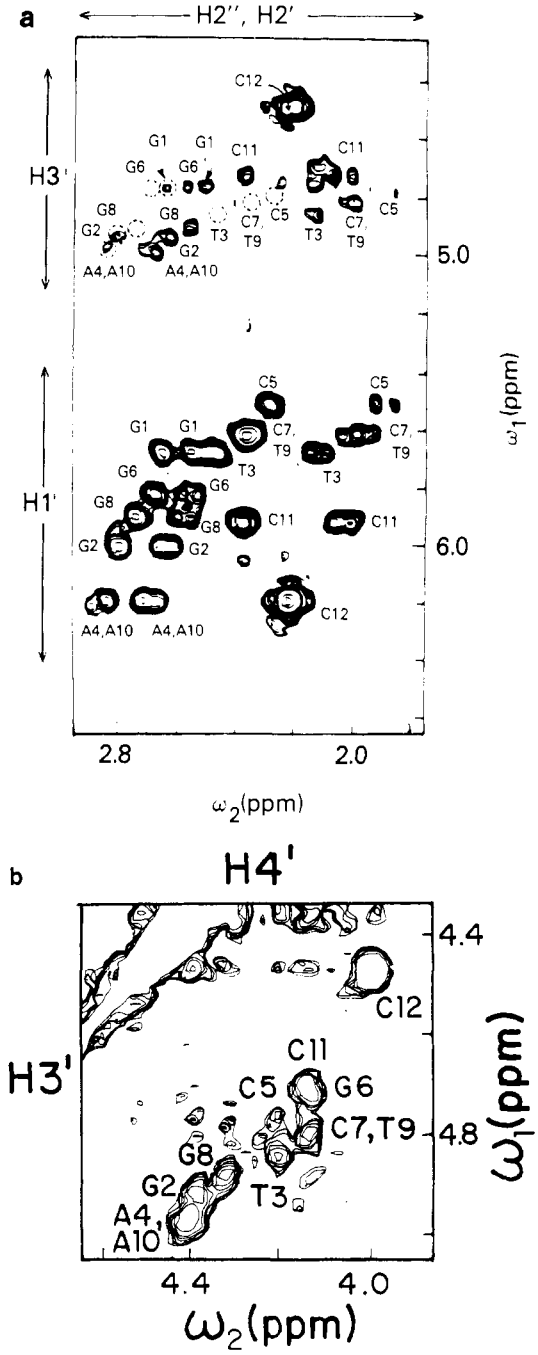

FIGURE 9: Expansions of selected regions of the 500-MHz proton COSY spectrum of d-GGTACGCGTACC in ^2H_2O at 25 °C. (a) This panel contains all the expected J-coupling correlations between H1′–H2′, H1′–H2″, H2′–H3′, and H2″–H3′. The absent and very weak H2″–H3′ cross peaks [J(H2″–H3′) = small] are shown with circles in their expected region. (b) This panel contains all the expected J-coupling correlations between H3′–H4′. The H3′–H4′ cross peak belonging to G1 could not be identified.

to smaller dispersions in both the H3′ and the H4′ chemical shifts (Figure 9b), quantification of these J values is again difficult. However, qualitative inferences on the magnitudes of J(H2′–H3′) and J(H3′–H4′) can be made from the intensities of the corresponding cross peaks in the low-resolution COSY spectrum.

Conformation of the Deoxyribose Rings. As discussed earlier, the experimental patterns of the phase-sensitive COSY multiplets in the H1′–H2′ and H1′–H2″ regions permit quantitative measurements of three of the five conformation-dependent vicinal J values in the individual deoxyribose rings of the oligonucleotide VI. The patterns are highly suggestive of a sugar geometry in the S domain of the pseudorotational conformation map lying close to O4′-endo. A qualitative estimate of the other two couplings J(H2′–H3′) and J(H3′–H4′) can be obtained from the low-resolution COSY spectrum. Such spectra are shown in panels a and b of Figure 9. The features are listed in Table II in terms of the intensities of the cross peaks. It may be noted first that, as already inferred from the phase-sensitive data, the values of J(H2″–H3′) are small and result in weak cross peaks or a complete absence of cross peaks in the low-resolution COSY spectrum. On the other hand, the peaks corresponding to H2′–H3′ are weak to medium. Thus, in the region corresponding to (H2′/H2″)–H3′ cross peaks (Figure 9a), only one of the two cross peaks is observed. The cross peaks corresponding to H3′–H4′ scalar correlations are moderately strong (Figure 9b), the only exception being G12 where such a peak could not be seen.

It is thus seen that though we are not able to make quantitative estimates, the values of both H2′–H3′ and H3′–H4′ couplings are moderately large. It is this important result which helps in precisely determining the sugar geometry and in distinguishing among the various conformers in the S domain. It is easy to see that except for G1, G2, C11, and C12, which are the terminal residues, the sugar conformations of the other deoxyribose rings lie between O4′-endo (P = 90°) and C1′-exo (P = 126°). The C2′-endo geometry which has been extensively used in fiber diffraction based models for B-DNA can be ruled out since the value of J(H3′–H4′) corresponding to this structure is 0 Hz, rather than the moderately large values observed here.

The conformation of G1 differs from the general pattern outlined above. The J value corresponding to H1′–H2′ in this case lies close to the maximum value expected for this coupling and would indicate a conformation between C1′-exo and C2′-endo. This is also consistent with the absence of a COSY cross peak in the H3′–H4′ spectral region and a somewhat lower value for J(H1′–H2″) compared to other nucleotides.

The case of C12 is complicated by the fact that in this case H2′ and H2″ have almost identical chemical shifts. The general behavior of the intensity patterns leads us to believe that the conformation is to the left of O4′-endo (P = 72°–90°). In the case of C11, phase-sensitive COSY suggests a behavior similar to the nucleotides T3 to A10. However, the low-resolution COSY shows a peak of medium intensity corresponding to J(H2″–H3′). Likewise, G2 shows a weak intensity for this peak.

In studies on solution conformations of nonhelical mono- and dinucleotides, the NMR coupling constant data have often been interpreted in terms of a dynamic equilibrium between C2′-endo (or S domain) and C3′-endo (N domain) sugar puckers (Govil & Hosur, 1982). While a fast equilibrium on the NMR time scale between these two widely different conformers is unlikely in double-helical DNA, the proposition is nevertheless attractive since the two conformations form the basis of models for A and B forms of DNA. The observed values of J(H1′–H2′), J(H1′–H2″), and J(H2″–H3′) may still be explained if a small contribution of C3′-endo conformer (less than 20%) is allowed with the C2′-endo as the major conformation. However, in such a situation, the time-average value of J(H3′–H4′) will be less than 2 Hz, which cannot explain the observation of H3′–H4′ cross peaks of sizable intensities in the low-resolution COSY spectrum. In fact, none of the possibilities involving equilibrium between two widely different conformations can explain the observed data in Table II. It thus seems that the molecular dynamics of the DNA

segment GGTACGCGTACC is confined within narrow regions of the sugar pucker in the S domain. It is possible that the terminal sugars G1, G2, C11, and C12 are relatively more flexible and show wider dynamical swings around their mean conformations compared to T3–A10.

Estimation of Intra- and Internucleotide Proton–Proton Distances (r). The use of homonuclear NOESY spectroscopy in structural determination is based on the fact that the main relaxation mechanism for protons is the dipole–dipole interactions between proton spins in close proximity. At mixing times which are short enough to neglect contributions from spin diffusion, the volumes (V_{ij}) of the NOESY cross peaks are proportional to the cross relaxation rates σ_{ij} (Kalk & Berendsen, 1976; Wagner & Wüthrich, 1979). The cross relaxation rates are, in turn, inversely proportional to the sixth power of the distance between the two protons interacting through a dipole–dipole interaction:

$$V_{ij} \propto \sigma_{ij} = f(\omega,\tau_c,\tau_m) r_{ij}^{-6} \quad (1)$$

where $f(\omega,\tau_c,\tau_m)$ is a function of the correlation time (τ_c), the mixing time (τ_m), and the spectrometer frequency (ω). Under conditions of slow motion ($\omega\tau_c \gg 1$), which is the case with biological molecules, a simplification arises, and the volumes are given by (Ernst et al., 1987)

$$V_{ij} \propto \tau_c \tau_m r_{ij}^{-6} \quad (2)$$

Assuming that the correlation time is the same for all proton pairs, an assumption which is fairly valid for nucleic acids, one obtains eq 3 for ratios of interproton distances.

$$V_{ij}/V_{kl} = (r_{kl}/r_{ij})^6 \quad (3)$$

If therefore one can choose a reliable standard distance in the molecule under study, then other proton–proton distances can be estimated from the relative volumes of the NOESY cross peaks.

Quantitative estimation of the proton–proton distances requires as a precondition estimation of the spin-diffusion limits which may be different for different protons. For example, sugar protons may have lower spin-diffusion limits compared to the base protons. Therefore, we have recorded NOESY spectra for VI using several mixing times, namely, 50, 75, 100, 150, 200, and 300 ms. The spectral sets have been used to estimate the volumes of the NOESY cross peaks at different mixing times with the relation

$$V = \pi L_1 L_2 h \quad (4)$$

where L_1 and L_2 are the half line widths at the half-heights along the ω_1 and ω_2 axes, respectively, and h is the height of the peak. Each peak is assumed to have a Lorentzian-absorptive line shape along both axes, which is a valid assumption when weak apodization functions are used for data manipulation. In order to measure L_1 and L_2 of the cross peaks, respective rows and columns have been plotted from spectra at all mixing times, retaining the same normalization constants during the two-dimensional Fourier transformations.

Figure 10 shows the buildup of some of the NOE volumes (Wagner & Wüthrich, 1979; Kumar et al., 1981) for intra- and internucleotide cross peaks in oligonucleotide VI. No attempts have been made to fit the data to any theoretical models. The different shapes of the NOE buildup curves arise from the locally different spin-diffusion rates, which in turn reflect on the locally different geometries. It is observed that even at 100 ms the curves become nonlinear, indicating small but finite contributions from spin-diffusion in the system. With mixing times of 50 ms and lower, the volume estimation of the NOESY cross peaks is highly inaccurate because of the low intensities of the resonance features. Therefore, NOESY

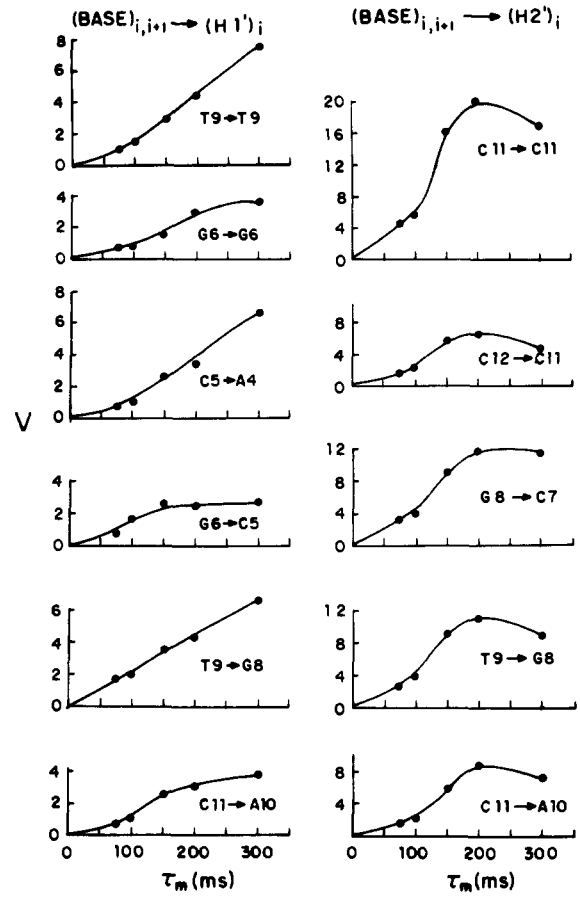

FIGURE 10: Buildup of normalized volumes of some intranucleotide and internucleotide NOESY cross peaks in d-GGTACGCGTACC as a function of mixing time.

spectra with a mixing time of 75 ms have been used for estimation of interproton distances.

In all these estimations we have used the thymine H6–CH3 distance of 3.00 Å as a reference. It may be pointed out that in DNA there are two other fixed distances, namely, H5–H6 (r = 2.45 Å) and H2′–H2″ (r = 1.85 Å), which can also be used as standards in distance measurements. However, both of the proton pairs have fairly large scalar couplings (8 and 14 Hz, respectively). At the short mixing times used in our work for obtaining dipolar interactions (75 ms), the J coupling correlations may contribute significantly to the NOESY cross peaks corresponding to these two pairs of protons. Use of H5–H6 and H2′–H2″ as standards may therefore lead to a wrong estimation of the unknown distances. This was indeed the case when we recalibrated the peaks using the H5–H6 cross peak as reference. The estimated distances were smaller by about 0.3–0.5 Å.

Furthermore, when the ratio of the coupling constant J between two nuclei is comparable to the corresponding chemical shift difference, then the basic spin wave functions are mixed, and it is no longer possible to regard a particular NOESY peak as arising purely from an interaction between two nuclei (Kay et al., 1986; Keeler et al., 1987). From this viewpoint, the worst case in oligonucleotides arises from the small chemical shifts between the H2′ and H2″ protons combined with their larger scalar couplings of around −14 Hz. In the case of the present oligonucleotide, apart from the two terminal nucleotides G1 and C12, the J/δ ratios are less than 0.2, and hence, such strong coupling effects are unlikely to influence the results.

The accuracy of the distance estimation is connected with the accuracy of the volume estimation of the cross peaks.

Table III: Intranucleotide Nonexchangeable Proton–Proton Distances (in Angstroms) in d-GGTACGCGTACC at 25 °C[a]

	G	G	T	A	C	G	C	G	T	A	C	C
H8/H6–H1′		3.9	3.6		3.6	3.7	3.7	3.6	3.6		3.9	
H8/H6–H2′		2.6	2.7		2.6	2.6	2.6	2.5	2.8		2.8	
H8/H6–H2″		3.6	3.7						3.7		3.9	

[a] The error in the estimation is ±0.2 Å. The blanks are the result of NOE cross peak overlap.

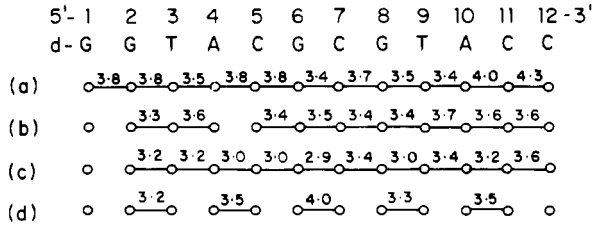

FIGURE 11: Measured internucleotide interproton distances between nonexchangeable base and sugar protons: (a) $(base)_{i+1}$–$(H1')_i$ (d_2); (b) $(base)_{i+1}$–$(H2')_i$ ($d_{3'}$); (c) $(base)_{i+1}$–$(H2'')_i$ ($d_{3''}$); (d) $(base)_{i+1}$–$(base)_i$ (d_1). The distances are accurate to ±0.2 Å.

However, because of the sixth power dependence of volumes on distances, a 20% error in volume estimation is found to affect distances only to the extent of 0.2 Å. Errors in volume estimation arise due to the following reasons: (i) insufficient digital resolution; (ii) apodization functions distorting line shapes; (iii) linewidth L_1 often limited by poor resolution in the spectrum, which in turn is due to a limited number of data points along t_1; (iv) poor S/N ratio; (v) insufficient repetition time between scans; (vi) "t_1–noise" overriding peaks. The reliability of distance estimates from volume measurements is also connected with the motions in the molecules. In the event of excessively fast motions, the distances are likely to be overestimated. There will also be inconsistencies in the relative distances, and such situations would point to conformational equilibria. In the present case, all the measured distances show internal consistencies with the proposed geometries along the length of the molecule.

Following the method mentioned above, 55 interproton distances have been measured in VI. Figure 11 shows the estimated internucleotide distances d_1, d_2, and d_3, namely, those between the base H8/H6 protons of residue $i + 1$ and the base and sugar protons H1′/H2′/H2″ of residue i. The internucleotide distances are given in Table III. The blanks in Figure 11 and Table III are due to extensive overlaps of the corresponding NOESY cross peaks which interfere with precise measurements of volumes. The magnitudes of the distances reported in Figure 11 and Table III and the labels on the observed NOEs suggest that the oligomer is a right-handed duplex, presumably B-DNA.

Glycosidic Dihedral Angle. The intranucleotide distances between the base (H6/H8) and the sugar protons depend both on the sugar pucker and the glycosidic dihedral angle (χ). Since in the present case the sugar pucker has already been determined as close to O4′-endo, it is possible to use the intranucleotide base to sugar distances to measure the angle χ. For example, Figure 12 shows the calculated intranucleotide distances between the base (H8/H6) and sugar (H1′, H2′, H2″, H3′, and H4′) protons as a function of χ for the O4′-endo geometry. Similar calculations have been reported earlier for other sugar geometries (Nanda et al., 1974; Wüthrich, 1986). It is clear from this figure that the base (H8/H6) distance from the H4′ proton is more than 4.3 Å for all values of χ. Hence, this distance will not give rise to NOESY cross peaks below the spin-diffusion limits. However, other distances vary widely in the range 1.5–6.0 Å and are very sensitive to the χ value. Therefore, these distances can be utilized to fix the glycosidic dihedral angle. In the present analysis, we have

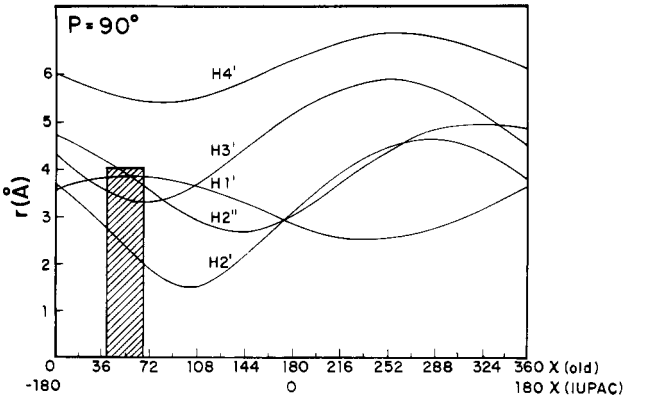

FIGURE 12: Plots of variation of different intranucleotide base (H8/H6) to sugar interproton distances as a function of glycosidic dihedral angle χ with O4′-endo sugar pucker. The shaded area depicts the preferred region in 8 out of the 12 nucleotides in d-GGTACGCGTACG. The two scales along the χ axis corresponds to the two widely followed conventions for measuring angles. On the top, the χ angle is measured along O4′–C1′–N1–C6 for pyrimidines and O4′–C1′–N9–C8 for purines. At the bottom, the χ angle is measured along O4′–C1′–N1–C2 for pyrimidines and O4′–C1′–N9–C4 for purines. In our previous work, we have followed the convention at the top. In the text of this work, we have adopted the lower conventions following IUPAC recommendations. The conventions differ by 180°. Likewise, the O1′ atom in the old convention has been relabeled as O4′ in this paper.

utilized the distances between the base (H8/H6) proton and the sugar H1′, H2′, and H2″ protons to obtain the value of χ. Distances involving H3′ could not be estimated because of the lower dispersions among the spectral features in this region of the NOESY spectrum.

In the case of G2, T3, T9, and C11, all the three distances have been estimated. In these four cases, the H8/H6–H1′ distances are in the range 3.6–3.9 Å. The H8/H6–H2′ distances are in the range 2.5–2.8 Å, and the r(H8/H6–H2″) values are 3.6–3.9. In the case of the C5, G6, C7, and G8 units, though we have not been able to estimate r(H6/H8–H2″), the H6/H8–H1′ and the H6/H8–H2′ distances provide sufficient information to fix the χ values. In these nucleotides, the base to H1′ and the base to H2′ distances are in the range 3.6–3.7 and 2.6–2.8 Å, respectively. From these distance estimates, it is possible to conclude that the χ values are centered around −130 ± 15°. The observations are indicated by the shaded region in Figure 12. In the case of G1, A4, A10, and C12, no intranucleotide base to sugar proton–proton distances could be measured because of signal overlaps and the end effects. Hence, the χ values could not be estimated.

It may be mentioned that in A-DNA, the χ values have been found to be around −155°, both from fiber and from single-crystal data (Arnott et al., 1980; Kennard, 1985). A somewhat larger deviation is observed in B-DNA. The average values are reported to be −102° from fiber data (Arnott et al., 1980). In the crystal structure of CGCGAATTCGCG (Dickerson & Drew 1981), the χ values span the range −90 to −135° and show a strong correlation with the sugar pucker. For O4′-endo geometries, the observed χ values are close to −125°.

Comparison of the Conformation of d-GGTACGCGTACC with DNA Models. In Table IV we compare the intra- and internucleotide proton–proton distances for A- and B-DNA

Table IV: Comparison of Intranucleotide and Internucleotide Distances between Nonexchangeable Protons in d-GGTACGCGTACC with Those of Standard A-DNA and B-DNA

distance	A-DNA[a]	B-DNA[a]	d-GGTACGCGTACC
	Intranucleotide Distances		
H6–H1′	3.4	3.6	3.6–3.7
H8–H1′	3.6	3.8	3.6–3.9
H6–H2′	4.0	2.1	2.6–2.8
H8–H2′	4.5	2.5	2.6
H6–H2″	4.4	3.4	3.6–3.9
H8–H2″	4.5	3.5	3.7
	Internucleotide $i + 1 \rightarrow i$ Distances		
H6–H1′	4.6	3.5	3.4–4.0
H8–H1	4.6	3.6	3.4–3.8
H6–H2′	2.0	4.0	3.3–3.6
H8–H2′	2.1	3.8	3.4–3.6
H6–H2″	3.7	2.2	2.9–3.6
H8–H2″	3.9	2.1	3.2–3.4
CH_3–H8	3.4	3.8	3.2–3.5
H5–H6	3.9	3.9	4.0
H5–H8	3.8	3.9	3.5

[a] Wüthrich (1986).

as reported by Wüthrich (1986) with the observed distances for the present dodecamer. In general, the experimental distances show a reasonable correspondence with the estimated distances for a standard B-DNA structure. The striking exceptions are the distances of the base (H8/H6) protons to the H2′ proton within the same nucleotide unit and the distances between the H6/H8 protons of the ith + 1 nucleotide unit and the H2″ protons of the sugar unit in the preceding nucleotide (i). The first difference is solely a manifestation of the differences in the sugar pucker present in VI (i.e., close to O4′-endo) and that used in the B-DNA model (close to C2′-endo). The second difference is a combined result of different torsional angles in the sugar–phosphate backbone, including the sugar pucker.

While such comparisons are interesting, it is important to realize that the standard geometries employed by Wüthrich are based on the fiber data and do not take into account sequence-specific effects. One of the important differences between the A and the B forms is in the conformation of the sugar ring. The models generally use a conformation close to C3′-endo for the A form and C2′-endo or a geometry close to it for the B form (Arnott et al., 1980; Govil & Hosur, 1982). Recent crystal structure data on a number of oligonucleotides which have been crystallized in the A form confirm that the conformation is fairly narrowly confined (average deviations are less than 20° in backbone dihedral angles for the A-DNA) and the sugar pucker is close to C3′-endo (Kennard, 1985). On the other hand, the B-DNA shows much wider sequence-dependent variations. For example, in the crystal structure of CGCGAATTCGCG (Dickerson & Drew, 1981), the sugar geometries show sequence-dependent variations ranging from C3′-endo to C2′-endo. The NMR data from our own laboratories for the molecules I–V listed in the introduction and those reported by others also indicate that the B-DNA can adopt much wider sequence-dependent conformational variations. In solutions, average sugar geometry is closer to O4′-endo than to C2′-endo (Hosur et al., 1986a,b, 1987b; Sheth et al., 1987a,b). The variations in the structure are not localized to the sugar pucker but are reflected in the other torsional angles, thereby altering the orientation of the phosphate groups and the relative positioning and stacking of the base pairs, which are the two important functional groups from the view of protein recognition.

In terms of establishing 3D geometry of DNAs by use of a sole NMR technique, it may be stated that the internucleotide distances shown in Figure 11 provide useful handles to determine the backbone dihedral angles. For example, the interbase distances, namely, G2 H8 → T3 CH_3, A4 H8 → C5 H5, G6 H8 → C7 H5, G8 H8 → T9 CH_3, and A10 H8 → C11 H5, indicate that the molecule is a right-handed helix. The number of measured internucleotide distances (four in most favorable cases) is not sufficient to uniquely fix the five backbone dihedral angles uniquely. However, even at this stage, it is evident from the variations in the distances that there are small but finite differences in the backbone dihedral angles along the sequence of the molecule.

It may be clear that compared to some of the other restriction enzyme binding sequences studied by us including the related oligomer GGATCCGGATCC, the present dodecamer exhibits a more uniform structure. In this case, the major structural variations are localized to the terminal residues G1, G2, C11, and C12. In addition, d_1 connectivities in the NOESY spectrum are found to be missing in certain segments (Figure 11d), implying somewhat larger base–base distances in these regions compared to those in B-DNA.

Conclusions

It has been our endeavor to develop the NMR methodology to obtain the maximum possible information on solution conformations of nucleic acids from the experimental methodologies of 2D NMR rather than to rely partly on energy minimization or molecular dynamics. At the level described in this paper, such a goal has been largely achieved. For example, we are able to fix the sugar geometries and the glycosidic bond dihedral angles. We can also obtain four sequential internucleotide (intrastrand) distances. Through imino proton resonances, the hydrogen-bond networks can be identified. For the A·T base pairs, it is also possible to measure some of the interstrand distances. With these additional constraints, it may be possible to work out the complete structures of nucleic acids entirely from NMR data.

Acknowledgments

The facilities provided by the 500-MHz FT NMR National Facility supported by the Department of Science and Technology and located at TIFR, Bombay, are gratefully acknowledged.

Registry No. VI, 113341-04-1.

References

Arnott, S., Chandrasekaran, R., Birdsall, D. L., Leslie, A. G. W., & Ratcliffe, R. L. (1980) *Nature (London) 283*, 743–746.

Atkinson, T., & Smith, M. (1984) in *Oligonucleotide Synthesis. A Practical Approach* (Gait, M. J., Ed.) IRL, Oxford.

Bax, A., & Freeman, R. (1981) *J. Magn. Reson. 44*, 542–561.

Chary, K. V. R., Hosur, R. V., Govil, G., Tan, Z., & Miles, H. T. (1987) *Biochemistry 26*, 1315–1322.

Chazin, W. T., Wüthrich, K., Hybert, S., Rance, M., William, A. D., & Leupin, W. (1986) *J. Mol. Biol. 190*, 439–453.

Clore, G. M., Gronenborn, A. M., & McLaughlin, L. W. (1985a) *Eur. J. Biochem. 151*, 153–165.

Clore, G. M., Gronenborn, A. M., Moss, D. S., & Tickle, I. J. (1985b) *J. Mol. Biol. 185*, 219–226.

Dickerson, R. E., & Drew, H. R. (1981) *J. Mol. Biol. 149*, 761–786.

Ernst, R. R., Bodenhausen, G., & Alexander, W. (1987) *Principles of Nuclear Magnetic Resonance in One and Two Dimensions*, pp 524–530, Clarendon, Oxford.

Feigon, J., Wright, J. M., Leupin, W., Denny, W. A., & Kearns, D. R. (1982) *J. Am. Chem. Soc. 104*, 5540–5541.
Feigon, J., Denny, W. A., Leupin, W., & Kearns, D. R. (1983a) *Biochemistry 22*, 5930–5942.
Feigon, J., Leupin, W., Denny, W. A., & Kearns, D. R. (1983b) *Biochemistry 22*, 5943–5951.
Frechet, D., Cheng, D. M., Kan, L. S., & Ts'o, P. O. P. (1983) *Biochemistry 22*, 5194–5200.
Govil, G., & Hosur, R. V. (1982) *Conformation of Biological Molecules: New Results from NMR*, Springer-Verlag, Heidelberg.
Hare, D. E., Shapiro, L., & Patel, D. J. (1986a) *Biochemistry 25*, 7445–7456.
Hare, D. E., Shapiro, L., & Patel, D. J. (1986b) *Biochemistry 25*, 7456–7474.
Hare, D. R., Wemmer, D. E., Chou, S. H., Drobny, G., & Reid, B. R. (1983) *J. Mol. Biol. 171*, 319–336.
Hore, P. J. (1983) *J. Magn. Reson. 55*, 283–300.
Hosur, R. V., Ravikumar, M., Roy, K. B., Tan, Z., Miles, H. T., & Govil, G. (1985a) in *Magnetic Resonance in Biology and Medicine* (Govil, G., Khetrapal, C. L., & Saran, A., Eds.) pp 243–260, Tata McGraw-Hill, New Delhi.
Hosur, R. V., Ravikumar, M., & Sheth, A. (1985b) *J. Magn. Reson. 65*, 375–381.
Hosur, R. V., Chary, K. V. R., Kumar, A., & Govil, G. (1985c) *J. Magn. Reson. 62*, 123–127.
Hosur, R. V., Chary, K. V. R., & Ravikumar, M. (1985d) *Chem. Phys. Lett. 116*, 105–108.
Hosur, R. V., Ravikumar, M., Chary, K. V. R., Sheth, A., Govil, G., Tan, Z., & Miles, H. T. (1986a) *FEBS Lett. 205*, 71–76.
Hosur, R. V., Sheth, A., Chary, K. V. R., Ravikumar, M., Govil, G., Tan, Z., & Miles, H. T. (1986b) *Biochem. Biophys. Res. Commun. 139*, 1224–1232.
Hosur, R. V., Chary, K. V. R., Majumdar, A., & Govil, G. (1987a) *Life Sci. Adv.* (submitted for publication).
Hosur, R. V., Chary, K. V. R., Sheth, A., Govil, G., & Miles, H. T. (1987b) *J. Biosci.* (in press).
Kalk, A., & Berendsen, H. J. C. (1976) *J. Magn. Reson. 24*, 343–366.
Kay, L. E., Scarsdale, J. N., Hare, D. R., & Prestegard, J. H. (1986) *J. Magn. Reson. 68*, 515–525.
Keeler, J., Neuhaus, D., & Williamson, M. P. (1987) *J. Magn. Reson. 73*, 45–68.
Kennard, O. (1985) *J. Biomol. Struct. Dyn. 3*, 205–226.
Kumar, A., Wagner, G., Ernst, R. R., & Wüthrich, K. (1981) *J. Am. Chem. Soc. 103*, 3654–3658.
Kumar, A., Hosur, R. V., & Chandrasekhar, K. (1984) *J. Magn. Reson. 60*, 143–148.
Marion, D., & Wüthrich, K. (1983) *Biochem. Biophys. Res. Commun. 113*, 967–974.
McBride, L. J., & Caruthers, M. H. (1983) *Tetrahedron Lett. 24*, 245–248.
Nanda, R. K., Tewari, R., Govil, G., & Smith, I. C. P. (1974) *Can. J. Chem. 52*, 371–375.
Ravikumar, M., Hosur, R. V., Roy, K. B., Miles, H. T., & Govil, G. (1985) *Biochemistry 24*, 7703–7711.
Reid, D. G., Salisbury, S. A., Bellard, S., Shakked, Z., & Williams, D. H. (1983) *Biochemistry 22*, 2019–2025.
Rinkel, L. J., & Altona, C. (1987) *J. Biomol. Struct. Dyn. 4*, 621–649.
Scheek, R. M., Russo, N., Boelens, R., Kaptein, R., & van Boom, J. H. (1983) *J. Am. Chem. Soc. 105*, 2914–2916.
Scheek, R. M., Boelens, R., Russo, N., Van Boom, J. H., & Kaptein, R. (1984) *Biochemistry 23*, 1371–1376.
Sheth, A., Ravikumar, M., Hosur, R. V., Govil, G., Tan, Z., & Miles, H. T. (1987a) *Biochem. Biophys. Res. Commun. 144*, 26–34.
Sheth, A., Ravikumar, M., Hosur, R. V., Govil, G., Tan, Z., Roy, K. B., & Miles, H. T. (1987b) *Biopolymers 26*, 1301–1313.
Sinha, N. D., Biernat, J., McManus, J., & Kaster, H. (1984) *Nucleic Acids Res. 12*, 4539–4557.
Staehelin, M., Sober, H. A., & Peterson, E. A. (1959) *Arch. Biochem. Biophys. 85*, 289–291.
Tomlinson, R. V., & Tener, G. M. (1963) *Biochemistry 2*, 697.
Wagner, G., & Wüthrich, K. (1979) *J. Magn. Reson. 33*, 675–680.
Wüthrich, K. (1986) *NMR of Proteins and Nucleic Acids*, pp 203–220, Wiley-Interscience, New York.
Wynants, C., & Van Binst, G. (1984) *Biopolymers 23*, 1799–1804.